Neurocomputing 128 (2014) 242–248

Contents lists available at ScienceDirect

Neurocomputing

journal homepage: www.elsevier.com/locate/neucom

Neural modeling of vapor compression refrigeration cycle with extreme learning machine

Lei Zhao [a], Wen-Jian Cai [a,*], Zhi-Hong Man [b]

[a] EXQUISITUS, Centre for E-City, School of Electrical and Electronic Engineering, Nanyang Technological University, Singapore 639798, Singapore
[b] Faculty of Engineering and Industrial Sciences, Swinburne University of Technology, Vic. 3122, Australia

ARTICLE INFO

Article history:
Received 7 September 2012
Received in revised form
27 February 2013
Accepted 20 March 2013
Available online 25 October 2013

Keywords:
Extreme learning machine
Vapor compression refrigeration cycle
Modeling
Back propagation
Support vector regression
Radial basis function

ABSTRACT

In this paper, a single-hidden layer feed-forward neural network (SLFN) is used to model the dynamics of the vapor compression cycle in refrigeration and air-conditioning systems, based on the extreme learning machine (ELM). It is shown that the assignment of the random input weights of the SLFN can greatly reduce the training time, and the regularization based optimization of the output weights of the SLFN ensures the high accuracy of the modeling of the dynamics of vapor compression cycle and the robustness of the SLFN against high frequency disturbances. The new SLFN model is tested with the real experimental data and compared with the ones trained with the back propagation (BP), the support vector regression (SVR) and the radial basis function neural network (RBF), respectively, with the results that the high degree of prediction accuracy and strongest robustness against the input disturbances are achieved.

1. Introduction

It is well known that the function of refrigeration and air-conditioning systems is to remove heat from one physical location to another. And it is essential in modern way of life to use these refrigeration equipments for the preservation of food, human comfort, the cooling of chemical and industry processes and so on [1]. In recent years, many engineering techniques have been employed for modeling vapor compression cycle (VCC) systems. Neural networks [2,3], due to their excellent performance in approximating complex nonlinear functions, have been introduced for modeling and optimizing air conditioning systems. Hosoz and Ertunc [4] developed a neural network model with five neurons in input layer for the system states and performance of a refrigeration system with an evaporative condenser. Yilmaz and Atik [5] proposed a feed-forward neural network with condenser water flow rate as the input to predict the performance of a variable cooling capacity mechanical cooling system. Navarro et al. [6] developed a radiant based function neural network model for predicting the performance parameters (such as cooling capacity, power consumption and chiller water outlet temperature) of a variable speed compression based refrigeration systems.

Recently, a novel learning algorithm for single-hidden-layer feed-forward neural networks (SLFN), called extreme learning machine (ELM), has been developed in [7–12] by Huang et al. The main characteristics of the ELM are that both the input-weights and hidden biases are randomly chosen, and the output weights are analytically determined by using the Moore–Penrose (MP) generalized inverse [13]. It has been further shown in [14] that ELM achieves the better generalization performance for equality constrained optimization problems, the extremely fast speed of convergence, and the easy conversion of complex learning into simple linear fitting. Most importantly, the ELM avoids many difficulties brought by gradient-based learning methods such as choosing stopping criteria, learning rate, learning epochs, local minima, and the over-tuned problems. ELM has been widely used in various fields due to its excellent speed and high accuracy. Nizar et al. [15] employed both ELM and online ELM to analyze the nontechnical loss and extracted customer behavior patterns with ELM as data mining techniques. Zhan et al. [16] applied ELM to investigate the relationship between sales amount and some significant factors which affect demand. The experiment results show that ELM outperforms back propagation in accuracy and speed. Kim et al. [17] proposed to use morphology filter and principle component analysis for feature extraction, and then used ELM to classify the ECG signal into six beat types, experiment results prove that its performance is better than that of BP, RBF and SVM.

In this paper, we will use an SLFN to model the dynamics of a vapor compression cycle. It will be shown that, with the ELM, the

* Corresponding author. Tel.: +65 6790 6862; fax: +65 6793 3318.
E-mail address: ewjcai@ntu.edu.sg (W.-J. Cai).

0925-2312/$ - see front matter © 2013 Elsevier B.V. All rights reserved.
http://dx.doi.org/10.1016/j.neucom.2013.03.058

Nomenclatures

A	opening percentage
F	frequency
H	enthalpy
P	pressure
Q	heat transfer rate
SH	superheat
SC	subcool
T	temperature
$\dot{W}$	power consumption
$\dot{m}$	mass flow rate
ω	compressor rotation speed

Subscripts

c	condenser
ca	condenser fan
e	evaporator
ea	evaporator fan
ev	expansion valve
i	inlet/*i*th group
in	indoor
o	outlet/outside
req	requirement
t	total

input weights are randomly assigned and the output weights are globally trained with the batch learning type least squares. In addition to the standard constraint used in the ELM, the constraint that satisfies the cooling load requirement in a vapor compression system is included in the global optimization for deriving the optimal output weights of the SLFN. In the experimental section, all training data pairs are obtained from the experiments, and the SLFN model is tested and compared with the ones trained with the BP, the SVR and the RBF, with the results that the developed SLFN model behaves with excellent robustness against high frequency noises involved in the testing data and provides the high accuracy for the prediction of the system states in the vapor compression cycle.

2. Introduction to vapor compression cycle

The vapor compression cycle system consists of the four main components: evaporator, compressor, condenser, and expansion valve, as shown in Fig. 1.

It is seen that these components are connected in a closed loop so that the working fluid can be continuously circulated in the system. The working principle of the vapor compression cycle is briefly described as follows [18]:

i. Initial temperature T of the liquid refrigerant inside the evaporator is lower than the temperature $T_{e,air,i}$ of the cold reservoir, and such a temperature difference makes the heat transfer from the reservoir to the refrigerant. The refrigerant will then evaporate after absorbing enough heat.
ii. After entering the compressor, the refrigerant vapor is compressed with high pressure, and such a process has also raised the refrigerant vapor's temperature.
iii. In the condenser, the heat of the refrigerant vapor is removed and the refrigerant vapor is condensed to liquid with the lower temperature.
iv. As soon as passing through the expansion valve, part of the refrigerant liquid evaporates, as its pressure is immediately reduced from the condensing pressure P_c to the evaporating pressure P_e, the heat absorption in evaporation process results in steep temperature decrease. Then the refrigerant enters the evaporator for the next cycle.

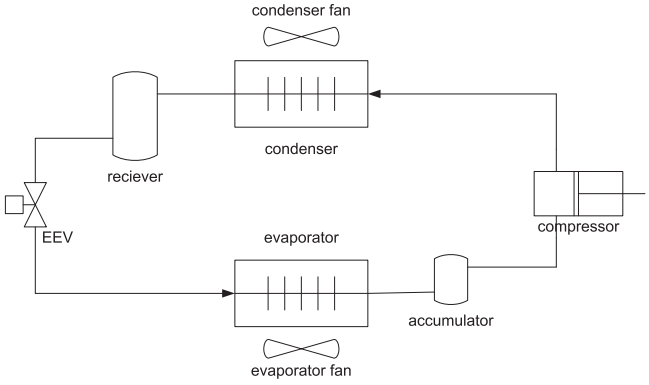

Fig. 1. Vapor compression refrigeration cycle.

3. Introduction to ELM

Consider N distinct sample data vector pairs (X_i, t_i) that are the collected measurements from a vapor compression cycle. The ith input pattern vector and the desired ith output vector are respectively defined as $X_i = [x_{i1} \quad x_{i2} \quad \dots \quad x_{in}]^T$ and $t_i = [t_{i1} \quad t_{i2} \quad \dots \quad t_{im}]^T$, for $i = 1, 2, \dots N$. The structure of SLFN to be used to learn the given input and output pairs is shown in Fig. 2 where the nodes in the input and output layer are linear, and the nodes in hidden layer are with the nonlinear activation functions, described by

$$y_{ki} = \varphi(W_k^T x_i) \tag{1}$$

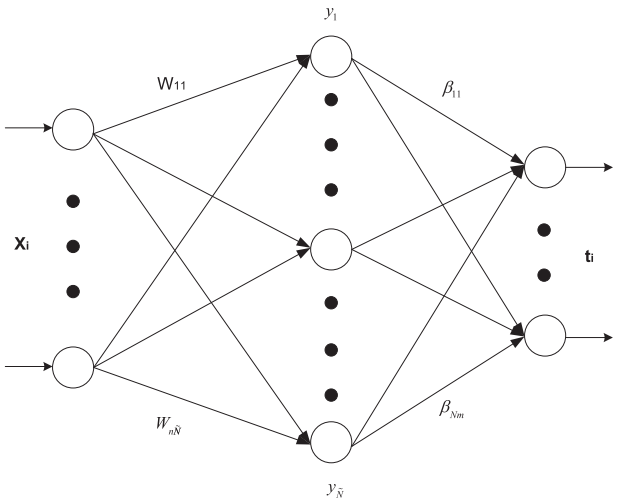

Fig. 2. Single hidden layer feed-forward neural network.

W_k in (1) is the input weight vector to the kth hidden neuron, defined as

$$W_k = \begin{bmatrix} W_{1k} & W_{2k} & \dots & W_{nk} \end{bmatrix}^T \tag{2}$$

for $k = 1, 2, \dots \tilde{N}$, and values of the input weights in W_k are all randomly selected based on ELM [7,12].

The hidden layer output vector Y_i, corresponding the input vector X_i, can then be expressed as

$$\begin{aligned} Y_i &= \begin{bmatrix} y_{1i} & y_{2i} & \dots & y_{\tilde{N}i} \end{bmatrix}^T \\ &= \begin{bmatrix} \varphi(W_1^T X_i) & \varphi(W_2^T X_i) & \dots & \varphi(W_{\tilde{N}}^T X_i) \end{bmatrix}^T \end{aligned} \tag{3}$$

Using (3), the jth output of the SLFN can be obtained as

$$O_{ji} = \sum_{l=1}^{\tilde{N}} \beta_{lj} \varphi(W_l^T X_i) \quad j = 1, 2, \dots m \tag{4}$$

and the ith output vector of the SLFN is of the form

$$\begin{aligned} O_i &= \begin{bmatrix} O_{1i} & O_{2i} & \dots & O_{mi} \end{bmatrix}^T \\ &= \begin{bmatrix} \sum_{l=1}^{\tilde{N}} \beta_{l1} \varphi(W_l^T X_i) & \sum_{l=1}^{\tilde{N}} \beta_{l2} \varphi(W_l^T X_i) & \dots & \sum_{l=1}^{\tilde{N}} \beta_{lm} \varphi(W_l^T X_i) \end{bmatrix}^T \end{aligned} \tag{5}$$

Then all N output vectors of the SLFN, corresponding to the N distinct input vectors $X_1, X_2 \dots X_N$, can be written in the following matrix form

$$\begin{aligned} O &= [O_1 \quad O_2 \dots O_N] \\ &= \begin{bmatrix} \sum_{l=1}^{\tilde{N}} \beta_{l1} \varphi(W_l^T X_1) & \sum_{l=1}^{\tilde{N}} \beta_{l1} \varphi(W_l^T X_2) & \dots & \sum_{l=1}^{\tilde{N}} \beta_{l1} \varphi(W_l^T X_N) \\ \vdots & \vdots & \dots & \vdots \\ \sum_{l=1}^{\tilde{N}} \beta_{lm} \varphi(W_l^T X_1) & \sum_{l=1}^{\tilde{N}} \beta_{lm} \varphi(W_l^T X_2) & \dots & \sum_{l=1}^{\tilde{N}} \beta_{lm} \varphi(W_l^T X_N) \end{bmatrix} \\ &= \begin{bmatrix} \beta_1^T \phi_1 & \beta_1^T \phi_2 & \dots & \beta_1^T \phi_N \\ \beta_2^T \phi_1 & \beta_2^T \phi_2 & \dots & \beta_2^T \phi_N \\ \vdots & \vdots & \vdots & \vdots \\ \beta_m^T \phi_1 & \beta_m^T \phi_2 & \dots & \beta_m^T \phi_N \end{bmatrix} = \beta^T \phi \end{aligned} \tag{6}$$

with

$$\beta_i = \begin{bmatrix} \beta_{1i} & \beta_{2i} & \dots & \beta_{\tilde{N}i} \end{bmatrix}^T \quad i = 1, 2, \dots m \tag{7}$$

$$\phi_i = \begin{bmatrix} \varphi(W_1^T X_i) & \varphi(W_2^T X_i) & \dots & \varphi(W_{\tilde{N}}^T X_i) \end{bmatrix}^T \quad i = 1, 2, \dots N \tag{8}$$

$$\beta = \begin{bmatrix} \beta_1 & \beta_2 & \dots & \beta_m \end{bmatrix} \tag{9}$$

$$\phi = \begin{bmatrix} \phi_1 & \phi_2 & \dots & \phi_N \end{bmatrix} \tag{10}$$

4. SLFN modeling of VCC

For the modeling of the dynamics of VCC, the input and the output vectors are chosen as

$$X_i = \begin{bmatrix} \omega_i & F_{eai} & F_{cai} & A_{vi} & T_{outi} & T_{ini} \end{bmatrix}^T \tag{11}$$

and

$$t_i = \begin{bmatrix} P_{ci} & P_{ei} & SC_i & SH_i & W_{ii} \end{bmatrix}^T \tag{12}$$

for $i = 1, 2, \dots N$, where ω, F_{ea}, F_{ca}, A_v, T_{out} and T_{in} are compressor rotation speed, evaporator fan frequency, condenser fan frequency, expansion valve opening percentage, outdoor temperature and indoor temperature, respectively. P_c, P_e, SC, SH and W are condensing pressure, evaporating pressure, subcool, superheat and system power consumption, respectively.

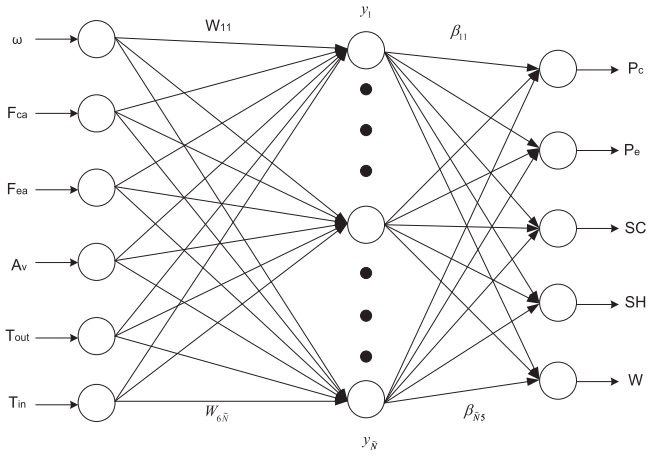

Fig. 3. The SLFN for modeling of VCC dynamics.

The following SLFN in Fig. 3 will be used to model the dynamic relationship between the input vectors and the output vectors described in (11) and (12), respectively.

It is seen from the above descriptions that, after the input weights are randomly initialized, the accuracy of the modeling of the VCC dynamics largely depends on the values of the output weights of the SLFN. For this purpose, we formulate the optimization problem of the output weight matrix β as follows:

$$\min \left\{ \frac{1}{2} \|\varepsilon\|^2 + \frac{d}{2} \|\beta\|^2 \right\} \tag{13}$$

subject to

$$\varepsilon = O - T = \beta^T \phi - T \tag{14}$$

and

$$Q_{ei} = Q_{rqi} = f(T_{out,i}, T_{in,i}) \quad i = 1, 2, \dots N \tag{15}$$

where matrix O in (14) contains all output data of the SLFN, corresponding the N input pattern vectors, as described in (5).

Remark 4.1:. The optimization constraint in (15) indicates that the VCC system must meet the cooling load requirement, which can be approximated to a function of indoor and outdoor temperature [19,20].

Based on the system dynamics, we can express Q_{ei} as follows:

$$\begin{aligned} Q_{ei} &= m_r * (H_{eo} - H_{co}) \\ &= \omega_i \left(c_{com,m,1} - c_{com,m,2} (P_{ci}/P_{ei})^{c_{com,m,3}} \right) (b_{he,1} + b_{he,2} P_{ei} + b_{he,3} SH_i \\ &\quad - (b_{hc,1} + b_{hc,2} P_{ci} + b_{hc,3} SC_i)) \end{aligned} \tag{16}$$

Defining

$$\gamma_i = \omega_i \left(c_{com,m,1} - c_{com,m,2} (P_{ci}/P_{ei})^{c_{com,m,3}} \right) \tag{17}$$

we can then rewrite Q_{ei} as follows:

$$\begin{aligned} Q_{ei} &= \gamma_i \bullet ((b_{he,1} - b_{hc,1}) - b_{hc,2} P_{ci} + b_{he,2} P_{ei} - b_{hc,3} SC_i + b_{he,3} SH_i) \\ &= d_{0i} + \begin{bmatrix} d_{1i} & d_{2i} & d_{3i} & d_{4i} & 0 \end{bmatrix} \begin{bmatrix} P_{ci} & P_{ei} & SC_i & SH_i & W_{ei} \end{bmatrix}^T \\ &= d_{0i} + d_i^T O_i \end{aligned} \tag{18}$$

where

$$\begin{cases} d_{0i} = \gamma_1 (b_{he,1} - b_{hc,1}) \\ d_{1i} = -\gamma_1 b_{hc,2} \\ d_{2i} = \gamma_1 b_{he,2} \\ d_{3i} = -\gamma_1 b_{hc,3} \\ d_{4i} = \gamma b_{he,3} \\ d_{5i} = 0 \end{cases}, \quad \beta_k = \begin{bmatrix} \beta_{1k} \\ \beta_{2k} \\ \vdots \\ \beta_{\tilde{N}k} \end{bmatrix} \quad \phi_p = \begin{bmatrix} \varphi(W_1^T X_p) \\ \varphi(W_2^T X_p) \\ \vdots \\ \varphi(W_{\tilde{N}}^T X_p) \end{bmatrix} = \begin{bmatrix} \phi_{1p} \\ \phi_{2p} \\ \vdots \\ \phi_{\tilde{N}p} \end{bmatrix} \tag{19}$$

For the minimization of (13), the following Lagrange function is constructed:

$$L=\frac{1}{2}\sum_{i=1}^{5}\sum_{j=1}^{N}\varepsilon_{ij}^2+\frac{d}{2}\sum_{i=1}^{5}\sum_{j=1}^{\tilde{N}}\beta_{ij}^2 + \sum_{k=1}^{5}\sum_{p=1}^{N}\lambda_{kp}(\beta_k^T\phi_p-t_{kp}-\varepsilon_{kp})+\sum_{p=1}^{N}\bar{\lambda}_p(Q_{ep}-f(T_{out,p},T_{in,p})) \quad (20)$$

It is noted from (18) that

$$\begin{aligned}\sum_{p=1}^{N}\bar{\lambda}_p(Q_{ep}-Q_{rqp})&=\sum_{p=1}^{N}\bar{\lambda}_p(d_{0p}+d_p^TO_p-f(T_{out,p},T_{in,p}))\\&=\bar{\lambda}^Td_0+\sum_{p=1}^{N}\bar{\lambda}_pd_p^TO_p-\bar{\lambda}^Tf(T_{out},T_{in})\\&=\bar{\lambda}^Td_0+\sum_{p=1}^{N}\bar{\lambda}_p\sum_{k=1}^{5}d_{kp}\beta_k^T\phi_p-\bar{\lambda}^Tf(T_{out},T_{in})\end{aligned} \quad (21)$$

where

$$d_0=\begin{bmatrix}d_{01} & d_{02} & \dots & d_{05}\end{bmatrix}^T$$

$$d_p=\begin{bmatrix}d_{1p} & d_{2p} & \dots & d_{5p}\end{bmatrix}^T$$

$$f(T_{out},T_{in})=\begin{bmatrix}f(T_{out,1},T_{in,1}) & f(T_{out,2},T_{in,2}) & \dots & f(T_{out,N},T_{in,N})\end{bmatrix}^T$$

$$\bar{\lambda}^T=\begin{bmatrix}\bar{\lambda}_1 & \bar{\lambda}_2 & \dots & \bar{\lambda}_N\end{bmatrix}$$

$$\lambda=\begin{bmatrix}\lambda_1\\ \lambda_2\\ \vdots\\ \lambda_5\end{bmatrix}=\begin{bmatrix}\lambda_{11} & \lambda_{12} & \dots & \lambda_{1N}\\ \lambda_{21} & \lambda_{22} & \dots & \lambda_{2N}\\ \vdots & \vdots & \vdots & \vdots\\ \lambda_{51} & \lambda_{52} & \dots & \lambda_{5N}\end{bmatrix} \quad (22)$$

Differentiating (21) with respect to β_{ij}, we have

$$\begin{aligned}\frac{\partial L}{\partial\beta_{ij}}&=d\beta_{ij}+\sum_{p=1}^{N}\lambda_{jp}\phi_{ip}+\sum_{p=1}^{N}d_{jp}\phi_{ip}\bar{\lambda}_p\\&=d\beta_{ij}+\begin{bmatrix}\lambda_{j1} & \lambda_{j2} & \dots & \lambda_{jN}\end{bmatrix}\begin{bmatrix}\phi_{i1}\\ \phi_{i2}\\ \vdots\\ \phi_{iN}\end{bmatrix}\\&\quad+\begin{bmatrix}\bar{\lambda}_1 & \bar{\lambda}_2 & \dots & \bar{\lambda}_N\end{bmatrix}d_{j1}K\begin{bmatrix}\phi_{i1}\\ \phi_{i2}\\ \vdots\\ \phi_{iN}\end{bmatrix}\\&=d\beta_{ij}+\tilde{\lambda}_j\bullet\tilde{\phi}_i^T+d_{j1}\bar{\lambda}^TK\tilde{\phi}_i^T=0\end{aligned} \quad (23)$$

where

$$K=\begin{bmatrix}K_1 & 0 & \dots & \dots\\ 0 & K_2 & \ddots & \dots\\ \dots & \ddots & \ddots & 0\\ \dots & \dots & 0 & K_N\end{bmatrix}_{N\times N} \quad (24)$$

$$K_i=\frac{d_{ji}}{d_{j1}}=\frac{\gamma_i}{\gamma_1} \quad (25)$$

$$\tilde{\phi}_i=\begin{bmatrix}\phi_{i1} & \phi_{i2} & \dots & \phi_{iN}\end{bmatrix} \quad (26)$$

and

$$\tilde{\lambda}_j=\begin{bmatrix}\lambda_{j1} & \lambda_{j2} & \dots & \lambda_{jN}\end{bmatrix} \quad (27)$$

Thus

$$d\beta_{ij}=-(\tilde{\lambda}_j+d_j\bar{\lambda}^TK)\phi_i^T \quad (28)$$

$$d\beta_j^T=d\begin{bmatrix}\beta_{1j} & \beta_{2j} & \dots & \beta_{\tilde{N}j}\end{bmatrix}=-(\tilde{\lambda}_j+d_j\bar{\lambda}^TK)\phi^T \quad (29)$$

$$d\beta^T=\begin{bmatrix}\beta_1^T\\ \beta_2^T\\ \vdots\\ \beta_5^T\end{bmatrix}=-\begin{bmatrix}\tilde{\lambda}_1+d_1\bar{\lambda}^TK\\ \tilde{\lambda}_2+d_2\bar{\lambda}^TK\\ \vdots\\ \tilde{\lambda}_5+d_5\bar{\lambda}^TK\end{bmatrix}$$

$$\phi^T=-\left(\lambda+\begin{bmatrix}d_1\bar{\lambda}^TK\\ d_2\bar{\lambda}^TK\\ \vdots\\ d_5\bar{\lambda}^TK\end{bmatrix}\right)\phi^T=-\left(\lambda+\begin{bmatrix}d_1\\ d_2\\ \vdots\\ d_5\end{bmatrix}\bar{\lambda}^TK\right)\phi^T \quad (30)$$

$$d\beta=-\phi\left[\lambda^T+K\bar{\lambda}\begin{bmatrix}d_1 & d_2 & \dots & d_5\end{bmatrix}\right] \quad (31)$$

In addition

$$\begin{aligned}\sum_{p=1}^{N}\bar{\lambda}_p(Q_{ep}-f(T_{out,p},T_{in,p}))&=\sum_{p=1}^{N}\bar{\lambda}_p(d_{0p}+d_p^TO_p-f(T_{out,p},T_{in,p}))\\&=\begin{pmatrix}\bar{\lambda}_1 & \bar{\lambda}_2 & \dots & \bar{\lambda}_N\end{pmatrix}\begin{bmatrix}d_{o1}+d_1^TO_1-f(T_{out,1},T_{in,1})\\ d_{o2}+d_2^TO_2-f(T_{out,2},T_{in,2})\\ \vdots\\ d_{oN}+d_N^TO_N-f(T_{out,N},T_{in,N})\end{bmatrix}\\&=\bar{\lambda}^Td_0+\sum_{p=1}^{N}\bar{\lambda}d_p^TO_p-\bar{\lambda}^Tf(T_{out},T_{in})\\&=\bar{\lambda}^Td_0+\sum_{p=1}^{N}\bar{\lambda}\sum_{k=1}^{5}d_{kp}(\varepsilon_{kp}+t_{kp})-\bar{\lambda}^Tf(T_{out},T_{in})\end{aligned} \quad (32)$$

Thus

$$L=\frac{1}{2}\sum_{i=1}^{5}\sum_{j=1}^{N}\varepsilon_{ij}^2+\frac{d}{2}\sum_{i=1}^{5}\sum_{j=1}^{\tilde{N}}\beta_{ij}^2+\sum_{k=1}^{5}\sum_{p=1}^{N}\lambda_{kp}(\beta_k^T\phi_p-t_{kp}-\varepsilon_{kp}) +\bar{\lambda}^Td_0-\bar{\lambda}^Tf(T_{out},T_{in})+\sum_{p=1}^{N}\bar{\lambda}_p\sum_{k=1}^{5}d_{kp}(\varepsilon_{kp}+t_{kp}) \quad (33)$$

Also

$$\frac{\partial L}{\partial\varepsilon_{ij}}=\varepsilon_{ij}+\lambda_{ij}+\bar{\lambda}_jd_{ij}=0 \quad (34)$$

Correspondingly, the value of ε_{ij} is

$$\varepsilon_{ij}=-(\lambda_{ij}+\bar{\lambda}_jd_{ij}) \quad (35)$$

$$\varepsilon_j=\begin{bmatrix}\varepsilon_{1j}\\ \varepsilon_{2j}\\ \vdots\\ \varepsilon_{5j}\end{bmatrix}=-\begin{bmatrix}\lambda_{1j}+\bar{\lambda}_jd_{1j}\\ \lambda_{2j}+\bar{\lambda}_jd_{2j}\\ \vdots\\ \lambda_{5j}+\bar{\lambda}_jd_{5j}\end{bmatrix} \quad (36)$$

$$\varepsilon=\begin{bmatrix}\varepsilon_1 & \varepsilon_2 & \cdots & \varepsilon_N\end{bmatrix}=-\lambda-\begin{bmatrix}\bar{\lambda}_1d_{11} & \bar{\lambda}_2d_{12} & \dots & \bar{\lambda}_Nd_{1N}\\ \bar{\lambda}_1d_{21} & \bar{\lambda}_2d_{22} & \dots & \bar{\lambda}_Nd_{2N}\\ \vdots & \vdots & \dots & \vdots\\ \bar{\lambda}_1d_{51} & \bar{\lambda}_2d_{52} & \dots & \bar{\lambda}_Nd_{5N}\end{bmatrix}$$

$$=-\lambda-\left(\begin{bmatrix}d_1\\ d_2\\ \vdots\\ d_5\end{bmatrix}\bar{\lambda}K\right) \quad (37)$$

Thus

$$d\beta=-\phi\varepsilon^T=\phi(\beta^T\phi-T)^T=\phi\phi^T\beta-\phi T^T \quad (38)$$

$$(\phi\phi^T-dI)\beta=\phi T^T\Rightarrow\beta=(\phi\phi^T-dI)^{-1}\phi T^T \quad (39)$$

The optimal estimate of the output weight matrix β derived in (39) can then be used in the SLFN in Fig. 3 for the prediction of the system state defined in the output vector in (12).

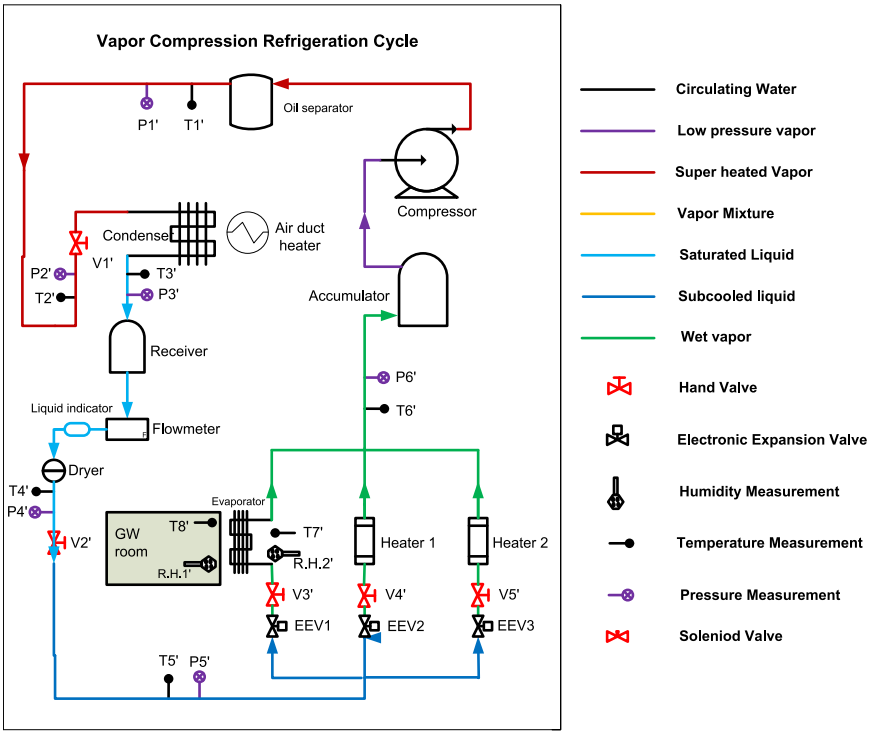

Fig. 4. Schematic of the vapor compression refrigeration system.

5. Experiment setup

In this experiment, we consider the vapor compression refrigeration system as described in Fig. 4.

The test bench consists of a semi-hermetic reciprocating compressor, an air-cooled finned-tube condenser, three electronic expansion valves and three evaporators (one air-cooled finned-tube evaporator and two electronic evaporators). One air duct heater controls the inlet air temperature of condenser for simulating outdoor condition, and the inlet air temperature of evaporator is constantly kept as 25 °C by HVAC system. The working fluid used for the system is R134a. The compressor, the condenser fan and the evaporator fan are equipped with inverters to adjust their corresponding frequencies. An air duct heater is installed in front of the condenser to control the temperature of condenser inlet air.

6. Performance evaluation

To illustrate the SLFN modeling for VCC dynamics proposed in this paper, we consider the SLFN with 50 hidden nodes, five output nodes and six input nodes, to model the measured system states with high frequency noise. Sigmoid function is chosen as the nonlinear function in hidden layer. The input data vectors to the SLFN are operating states under different cooling loads. The desired output reference values of the SLFN, providing with the desired values of the model, for all input data vectors, are measured through pressure, temperature sensors and power meter, respectively.

For comparison purpose, we have also implemented both the SLFNs, trained with the BP and the SVR, and the one whose hidden nodes are the RBFs, respectively. For the SLFN with the RBF hidden notes, the centers and widths of the RBFs are chosen randomly, the optimal output layer weights are calculated accordingly. Also, the cost parameters C and kernel parameters $\gamma$of SVR are 2^5 and 2^{-4}, respectively. One thousand data pairs are used for training all the SLFNs. To evaluate the generalization performance after training, the SLFN models are tested with 1000 groups of measured data disturbed with high frequency noises.

Both the measured values of the evaporating and condensing pressures and the predicted ones with SLFN are depicted in Fig. 5. It is seen that **(i)** the predicted deviation of the pressures obtained from the SLFN, trained with the ELM, is the smallest, and the corresponding prediction errors of P_c and P_e are almost within $\pm 4.5\%$ and $\pm 7\%$, respectively; **(ii)** the prediction errors of P_c and P_e from the SLFN with the hidden RBF nodes are slightly larger than the ones trained with the ELM; **(iii)** the prediction errors of SVR, on the other hand, are within $\pm 6\%$ and $\pm 10\%$, respectively; (**iv**) it is also noted that the deviations of the predicted value obtained from the SLFN with the BP are about $\pm 12\%$ and $\pm 17\%$, respectively.

Recall that it is preferable for the vapor to be slightly superheated for the purpose of compressor protection. According to the minimum stable signal (MSS) line proposed by Huelle [21], the temperature of the evaporator tube wall will fluctuate if superheat degree is below a certain value. Because of the 5 °C minimum superheat of the experiment system, both the SLFN training and testing set the range from 5 to 25 °C. Fig. 6 shows the predictions of the SH and the SC with the SLFNs trained with the ELM, the SVR and the BP, respectively, and the SLFN with the RBF hidden nodes trained with the ELM. It has been seen that the prediction deviations of both SH and SC obtained from the SLFN with the BP are the largest (11% and 20% respectively) and the prediction errors tend to increase as SH grows. It is also noted that the prediction errors of the SLFNs trained with the ELM and the SVR are within $\pm 7\%$. However, the prediction errors of the SLFN trained with the SVR also shows the trend of growth for large SH. In contrast, the performances of the SLFNs with both the sigmoid nonlinear hidden nodes and the RBF hidden nodes, trained with the ELM, are the best and stable in spite of a large testing range.

The energy consumption, as an output of the SLFN model, aims at identifying the sum of the energy consumptions of compressor, condenser and evaporator fans. It can be seen from Fig. 7 that the testing performance of the SLFN with BP is the worst compared

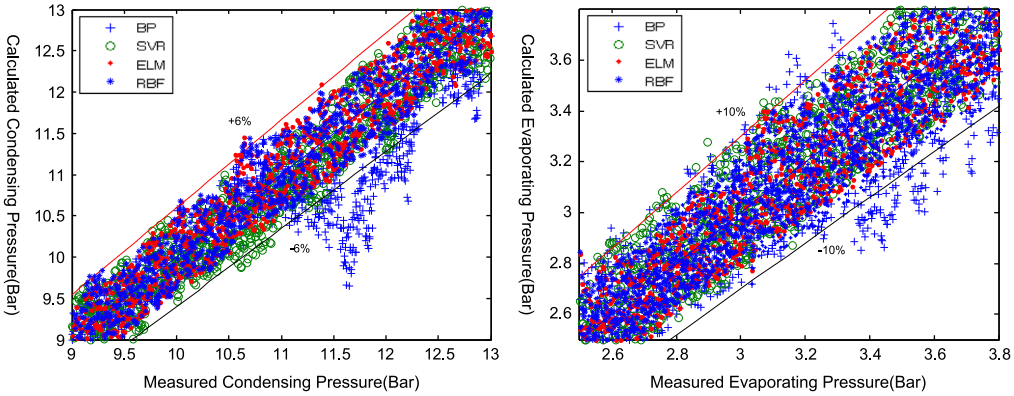

Fig. 5. P_c and P_e Testing Accuracy.

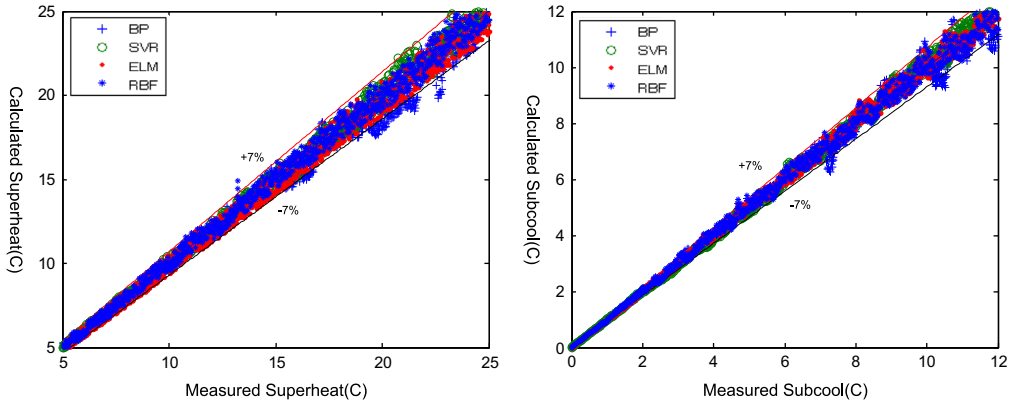

Fig. 6. *SH* and *SC* Testing Accuracy.

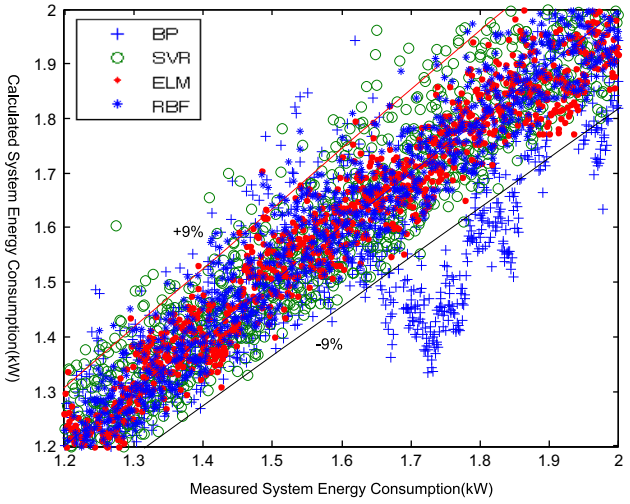

Fig. 7. W_t Testing Accuracy.

with the ones, trained with the SVR and the ELM, respectively. This is because the BP is based on the gradient decent method to search the global minimum in the weight space, and how to improve the robustness of the trained weights is not considered in the BP algorithm. In addition, for the SLFN with a large number of hidden nodes, the BP training can be easily trapped at some local minima. It can be further seen from the figure that, although the performance of the SLFN with the SVR is better than the one with the BP, the global optimization has made the SLFN trained with the ELM have the smallest the average RME, compared with the ones trained with the BP and the SVR. Another point noted from the figure is that the performance of the SLFN with the RBF hidden nodes is not stable, and the prediction error is large even when the system cooling load is small. Some further studies on the SLFN with the RBF hidden nodes for the VC modeling and analysis are under the authors' investigation.

Table 1
The comparison of training and testing accuracies.

Item (test)	BP		SVR		RBF		ELM	
	MSE	RME (%)	MSE	RME (%)	MSE	RME (%)	MSE	RME (%)
Pc	0.3828	2.77	0.2767	1.95	0.2487	1.74	0.2261	1.57
Pe	0.2387	5.65	0.1732	4.16	0.1479	3.25	0.1261	2.85
SH	0.6962	3.34	0.4237	2.71	0.3402	2.16	0.3193	1.91
SC	0.3363	2.53	0.2668	2.18	0.2587	2.01	0.2010	1.64
Wt	0.0929	7.56	0.0510	4.37	0.0489	4.10	0.0270	2.18

Table 2
Computation of training times.

Algorithm	Training time (s)	Testing time (s)
BP (30 hidden nodes)	12.2704	0.0622
SVR	15.7823	4.3642
RBF (50 hidden nodes)	0.0985	0.0528
ELM (50 hidden nodes)	0.0936	0.0570
ELM (200 hidden nodes)	0.1312	0.0624
ELM (500 hidden nodes)	0.5148	0.0980

Table 1 shows the comparisons of both the MSEs and RMEs of the SLFNs trained with the BP (with 30 hidden nodes), the SVR (C and γ are 2^5 and 2^{-4}), the RBF (50 hidden nodes with random Gaussian centers and spreads) and the ELM (with 500 hidden

nodes), respectively. It has been seen that the training time for the SLFN with the BP is the longest because of its recursive feature for the training both the input weights and the output weights. However, the training time of the SLFN with the ELM is only slightly larger than RBF, much less than BP and SVR. This point can be easily understood in the sense that no updating is needed for the randomly selected input weights or centers of the SLFN or RBF during the training.

Table 2 shows the comparisons of the training times as well as the testing times that are used for the SLFNs trained with the BP (30 hidden nodes), the SVR and the ELM (with 50, 200 and 500 hidden nodes), respectively. Obviously, the SLFN trained with the ELM performs the best.

7. Conclusion

In this paper, the modeling of the dynamics of vapor compression cycle with the SLFN has been studied. It has been seen that the SLFN model, trained with the ELM, can achieve the smallest modeling error and behave with a strong robustness against the input disturbances and system uncertainties. The testing and comparison results with the experimental data have further confirmed the excellent performance of the developed neural model.

Acknowledgments

The work was funded by National Research Foundation of Singapore: NRF2008EWT-CERP002-010. The other project partners are also acknowledged.

References

[1] W.B. Gosney, Principles of Refrigeration, Cambridge University Press, Cambridge [Cambridgeshire]; New York, 1982.
[2] S.S. Haykin, Neural Networks and Learning Machines, third ed., Prentice Hall, New York, 2009.
[3] G. Dreyfus, SpringerLink (Online service), Neural Networks Methodology and Applications, 2005.
[4] M. Hosoz, H.M. Ertunc, Artificial neural network analysis of a refrigeration system with an evaporative condenser, Appl. Ther. Eng. 26 (2006) 627–635.
[5] S. Yilmaz, K. Atik, Modeling of a mechanical cooling system with variable cooling capacity by using artificial neural network,, Appl. Ther. Eng. 27 (2007) 2308–2313.
[6] J. Navarro-Esbrí, V. Berbegall, G. Verdu, R. Cabello, R. Llopis, A low data requirement model of a variable-speed vapour compression refrigeration system based on neural networks,, Int. J. Refrig. 30 (2007) 1452–1459.
[7] G.-B. Huang, Q.-Y. Zhu, C.-K. Siew, Extreme learning machine: theory and applications,, Neurocomputing 70 (2006) 489–501.
[8] H. Guang-Bin, W. Dian Hui, L. Yuan, Extreme learning machines: a survey,, Int. J. Mach. Learn. Cybern. 2 (2011) 107–122.
[9] X. Cai, T.C. Yeh, Quantitative Information Fusion for Hydrological Sciences, Springer, Berlin, 2008.
[10] H. Guang-Bin, C. Lei, S. Chee-Kheong, Universal approximation using incremental constructive feedforward networks with random hidden nodes,, IEEE Trans. Neural Networks 17 (2006) 879–892.
[11] Z. Man, K. Lee, D. Wang, Z. Cao, C. Miao, A new robust training algorithm for a class of single-hidden layer feedforward neural networks, Neurocomputing 74 (2011) 2491–2501.
[12] H. Guang-Bin, Z. Qin-Yu, S. Chee-Kheong, Extreme learning machine: a new learning scheme of feedforward neural networks, in: Proceedings of the 2004 IEEE International Joint Conference on Neural Networks, Piscataway, NJ, USA, 25–29 July 2004, pp. 985–990.
[13] H. Ricardo, A Modern Introduction to Linear Algebra, CRC Press, Boca Raton, 2010.
[14] H. Guang-Bin, Z. Hongming, D. Xiaojian, Z. Rui, Extreme learning machine for regression and multiclass classification, IEEE Trans. Syst., Man Cyber., Part B (Cybernetics) 42 (2012) 513–529.
[15] A.H. Nizar, Z.Y. Dong, Y. Wang, Power utility nontechnical loss analysis with extreme learning machine method,, IEEE Trans. Power Syst. 23 (2008) 946–955.
[16] S. Zhan-Li, C. Tsan-Ming, A. Kin-Fan, Y. Yong, Sales forecasting using extreme learning machine with applications in fashion retailing, Decision Support Syst. 46 (2008) 411–419.
[17] K. Jinkwon, S. Hang Sik, S. Kwangsoo, L. Myoungho, Robust algorithm for arrhythmia classification in ECG using extreme learning machine, Biomed. Eng. OnLine 10 (2009) 31–42.
[18] R.J. Dossat, T.J. Horan, Principles of Refrigeration, fifth ed., Prentice Hall, Upper Saddle River, NJ, USA, 2002.
[19] American Society of Heating Refrigerating and Air-Conditioning Engineers and Knovel (Firm), ASHRAE Handbook Fundamentals (SI ed.) 2009.
[20] American Society of Heating Refrigerating and Air-Conditioning Engineers and Knovel (Firm), ASHRAE Handbook Heating, Ventilating, and Air-conditioning Systems and Equipment (Inch-Pound ed.) 2008.
[21] Z.R. Huelle, How to avoid evaporator system hunting in practice, Danfoss J. 26 (1971) 3–8.

Lei Zhao received the B.Eng. degree from Jilin University, China in 2008. He is currently a Ph.D. student with Control and Instrumentation Division, School of Electrical and Electronic Engineering, Nanyang Technological University, Singapore. His research interests include modeling and optimization of air conditioning and refrigeration system, neural network and intelligent algorithm. He has published a number of papers in international journals and conferences.

Wen-Jian Cai is currently in the School of EEE, Nanyang Technological University, since 1999. He received his B.Eng., M.Eng., and Ph.D. from Department of Precision Instrumentation Engineering, Department of Control Engineering, Harbin Institute of Technology, PR China, and Department of Electrical Engineering, Oakland University, USA, in 1980, 1983 and 1992, receptively. He has more than 20 years of industrial and research experience in the areas of mechanical design, system modeling and simulation, energy and environmental system automation, and process control. He participated in many industry related research projects, and published more than 100 technical papers, three books, two patents and received three national awards.

Zhi-Hong Man received his B.E. degree from Shanghai Jiaotong University, China, in 1982, M.Sc. degree from Chinese Academy of Sciences in 1987, and Ph.D. degree from the University of Melbourne, Australia, in 1994. From 1994 to 1996, he was the Lecturer in the School of Engineering, Edith Cowan University, Australia. From 1996 to 2001, he was the Lecturer and then the Senior Lecturer in the School of Engineering, The University of Tasmania, Australia. From 2002 to 2007, he was the Associate Professor of Computer Engineering at Nanyang Technological University, Singapore. From 2007 to 2008, he was the Professor of Electrical and Computer Systems Engineering, Monash University Sunway Campus, Malaysia. Since 2009, he has been the Professor of Engineering in the Faculty of Engineering and Industrial Sciences, Swinburne University of Technology, Australia. His research interests are in sliding mode control, signal processing, robotics, neural networks and electric vehicles.